

1 2 3 4 5 6 7 8

Towards deep learning-powered IVF: A large public benchmark for morphokinetic parameter prediction

Tristan Gomez

tristan.gomez@univ-nantes.fr

Magalie Feyeux

magalie.feyeux@univ-nantes.fr

Nicolas Normand

nicolas.normand@univ-nantes.fr

Laurent David

laurent.david@univ-nantes.fr

Perrine Paul-Gilloteaux

perrine.paul-gilloteaux@univ-nantes.fr

Thomas Fréour

thomas.freour@chu-nantes.fr

Harold Mouchère

harold.mouchere@univ-nantes.fr

March 2, 2022

*This work was funded by ANR - Next grant DL4IVF (2017)

†T. Gomez is with the University of Nantes, CNRS, LS2N, CNRS UMR 6004, F-44000 Nantes, France.

‡M. Feyeux is with the University of Nantes, Nantes University Hospital, Inserm, CNRS, SFR Santé, Inserm UMS 016, CNRS UMS 3556, F-44000 Nantes, France.

§N. Normand is with the University of Nantes, CNRS, LS2N, CNRS UMR 6004, F-44000 Nantes, France.

¶L. David is with the University of Nantes, Nantes University Hospital, Inserm, CNRS, SFR Santé, Inserm UMS 016, CNRS UMS 3556, F-44000 Nantes, France.

||P. Paul-Gilloteaux is with the University of Nantes, Nantes University Hospital, Inserm, CNRS, SFR Santé, Inserm UMS 016, CNRS UMS 3556, F-44000 Nantes, France.

**T. Fréour is with the University of Nantes, Nantes University Hospital, Inserm, CRTI, Inserm UMR 1064, F-44000 Nantes, France.

††H. Mouchère is with the University of Nantes, CNRS, LS2N, CNRS UMR 6004, F-44000 Nantes, France.

Abstract

An important limitation to the development of Artificial Intelligence (AI)-based solutions for In Vitro Fertilization (IVF) is the absence of a public reference benchmark to train and evaluate deep learning (DL) models. In this work, we describe a fully annotated dataset of 756 videos of developing embryos, for a total of 337k images. We applied ResNet, LSTM, and ResNet-3D architectures to our dataset and demonstrate that they overperform algorithmic approaches to automatically annotate stage development phases. Altogether, we propose the first public benchmark that will allow the community to evaluate morphokinetic models. This is the first step towards deep learning-powered IVF. Of note, we propose highly detailed annotations with 16 different development phases, including early cell division phases, but also late cell divisions, phases after morulation, and very early phases, which have never been used before. We postulate that this original approach will help improve the overall performance of deep learning approaches on time-lapse videos of embryo development, ultimately benefiting infertile patients with improved clinical success rates ¹

1 Introduction

Infertility is a global health issue worldwide [1]. The number of couples reporting infertility and referring to assisted reproductive technology (ART) centers for infertility workup and care in Europe is increasing by 8 - 9% every year [2]. One of the most common treatments for infertile couples is In Vitro Fertilization (IVF). It consists of controlled ovarian hyperstimulation, followed by ovum pickup, fertilization, and embryo culture for 2-6 days under controlled environmental conditions, leading to intrauterine transfer or freezing of embryos identified as having a good implantation potential by embryologists. The clinical effectiveness of IVF is variable across regions with reported efficiency ranging from 20% to 40%. IVF is mainly hampered by the current limitations of embryo quality assessment methods [3]. Indeed, the main embryo quality assessment method is based on morphological evaluation, which consists of daily static observation under the microscope. Although consensus exists for morphological evaluation of embryo development, this method still suffers from a lack of predictive power and inter- and intra-operator variability [4-6]. Time-lapse imaging incubators (TLI) were first released in the IVF market around 2010. They provide continuous monitoring of embryo development, by taking photographs of each embryo at regular intervals throughout its development, ultimately compiling a video giving a dynamic overview of embryonic in vitro development. This technology allows very stable culture conditions and leads to a dynamic annotation of embryonic developmental events, called morphokinetic (MK) parameters, such as, for instance, cell divisions, blastocyst formation, and expansion. Although several studies have reported an association between MK

¹Code and data are available at https://gitlab.univ-nantes.fr/E144069X/bench_mk_pred.git.

parameters and implantation potential, the clinical usefulness of TLI remains debated [7–9]. Nevertheless, TLI still appears to be the most promising solution to improve embryo quality assessment methods, and subsequently the clinical efficiency of IVF. In particular, the unprecedented high volume of high-quality images produced by TLI systems could be leveraged using modern Artificial Intelligence (AI) methods, like deep learning (DL). Indeed, the recent emergence of DL has revolutionized many fields like games [10], computer vision [11], language processing [12], protein folding [13], and its advent has set high expectations on its potential for medicine and biology and called for concrete applications. Importantly, the question of data sharing is at the center of DL strategies being applied to health data. Indeed, a model can not be reproduced and evaluated externally if the dataset used to train the model is not made available. The main reason behind this common absence of data sharing probably has to do with concerns about data security and maybe to a lesser extent with the made scientific competition. The consequence of a rather “black box” development of DL methods in IVF results in a lack of consensus about which DL architecture to use, with private companies selling and implementing solutions that have not been independently evaluated by the community, raising questions about potential bias and fairness issues for example [14]. Data sharing is therefore of utmost importance to properly implement DL in IVF practice [14]. In this context, we are in dire need of a reference time-lapse dataset and a baseline analysis with the most common DL algorithms, similar to what has been done in other fields [15–18]. Several teams have applied DL models in IVF, but with important limitations: either the number of videos was lower than 300 or the number of total images composing the videos was under 150k (table 1) [19–22].

Author	Year	Video nb.	Image nb.	Phases used	Accuracy obtained
Khan et al.	2016	256	150k	1-5 cells	87%
Moradi Rad et al.	2018	-	224	1-5 cells	82.4%
Silva-Rodríguez et al.	2019	263	100k	1-5 cel	80.9%
Kumar Kanakasabapathy et. al.	2019	-	8k	Blasto/No Blasto	96%
H Ng et al.	2018	-	600k	tStart to t4+	84.6%
Liu et al,	2019	170	60k	tStart to t4+	83.8%
Lau et al.	2019	1303	145k	tStart to t4+	83.65%

Table 1: Dataset characteristics of previous works.

Additionally, studies used a limited amount of embryonic stages / MK parameters to identify with DL. Finally, and as stated above, the studies did not share their datasets, making their analysis impossible to recapitulate. A shared dataset should be large enough to train powerful deep learning models, contain full videos to make full use of the TLI information, and have highly detailed annotations taking into account a large number of development phases to maximize potential clinical use. Here, we propose a unique reference benchmark that will allow the community to evaluate and compare morphokinetic models and

will be a step towards deep learning-powered IVF. The dataset contains 756 full videos and a total of 337k images which was sufficient to train and evaluate deep learning models. We applied ResNet, LSTM, and ResNet-3D architectures to our dataset and demonstrate that they overperform our previous algorithmic approach to automatically annotate stage development phases on TLI data [23]. Of note, we propose highly detailed annotations with 16 different development phases, from early cell division phases (t2-t5+) as in previous work, but also late cell divisions (t6 to t9+), phases after morulation (tM to tHB), and very early phases (tPNa and tPNf), which, to the best of our knowledge, have never been reported up to now.

2 Methods

2.1 Dataset collection

Between 2011 and 2019, 716 infertile couples underwent Intracytoplasmic Sperm Injection (ICSI) cycles in our University-based IVF center and had all their embryos cultured and monitored up to blastocyst stage with a TLI system. We randomly selected a subset of 873 videos, which is approximately 10% of all the videos recorded, because of the limited computational budget at the time of the study. We subsequently extracted all focal planes using an Application Programming Interface (API) provided by the TLI manufacturer (Vitrolife®). We acknowledge that only ICSI cycles were included in our time-lapse devices over that period, as we considered that conventional IVF would lead to different developmental timings as compared to ICSI. We do not routinely use assisted hatching. There were no major lab changes over the study period. The Local Institutional Review Board (GNEDS) approved this project. All patients agreed with the anonymous use of their clinical data. Patient treatment and embryo culture protocol were described in a previous study [24]. In brief, embryo culture was performed from fertilization (day 1) up to blastocyst stage (day 5 or day 6) at 37°C with 5% O₂ and 6% CO₂ in a sequential culture medium, i.e. G1 plus (Vitrolife®, Sweden) from day 0 to day 3, followed by G2 plus (Vitrolife®, Sweden). We acknowledge that culture media might impact embryo development and have an evolving composition throughout embryo development. However, the available literature does not support the concept of medium-dependent morphokinetic patterns [25]. Although we perfectly agree that there is a need to clarify IVF culture media composition to enhance our understanding of embryo development [26], there is no evidence to our knowledge that the content of commercial culture media changes over time in ways that are important enough to consider. The images were acquired with a TLI system (Embryoscope®, Vitrolife®, Sweden) every 10 to 20 min by a 1280 × 1024 resolution camera under a 635 nm LED light source passing through Hoffman’s contrast modulation optics. To reduce the noise in the annotations, we chose to keep only the videos showing at least 6 distinct stages of development to train and test our models. The final number of videos in our dataset is 756.

Among these videos, 526 correspond to embryos considered to be morphologically viable and subsequently chosen for transfer, while the other 230 videos correspond to discarded embryos because of poor development. The information about embryo viability is not used in this work as the purpose is to focus solely on morphokinetic parameter prediction. These discarded embryos allowed us to study a variety of abnormal embryonic features (abnormal morphology, abnormal fertilization/number of pro-nuclei, necrosis, fragmentation, developmental delay, etc.) or problems during image acquisition (sharpness, change of focus, brightness, etc.). All annotations on the videos were made by 2 qualified and experienced embryologists undergoing regular internal quality control. Annotations were made following the recommendations of Ciray et al. for the detection of stages [27], i.e. 16 phases corresponding to 16 cellular events: tPB2, tPNa, tPNf, t2, t3, t4, t5, t6, t7, t8, t9+, tM, tSB, tB, tEB and finally tHB [27]. Each phase refers to a specific cellular event i.e. polar body appearance for phase PB2 (pPB2), pronuclei appearance and disappearance (pPNa and pPNf), blastomere division from 2-cell stage to ≥ 8 cells-stage (p2 to p9+), compaction (phase pM), blastocyst formation (phases pSB, pB), expansion and hatching (phases pEB and pHB). We started prospective annotation of the database according to this reference work in 2014, while annotations made before 2014 were retrospectively checked. Although we included all available focal planes in the dataset, we only used the center focal plane in our experiments.

2.2 Models

Several baseline models were used to perform this classification task and compared using the defined metrics on the annotated dataset. The first model is designed for isolated image classification, the next two models allow the classification of images in a sequence. They are illustrated in fig. 1 and detailed below.

The ResNet Model. Residual models are widely used for the classification of isolated images, for example on ImageNet [28]. This model is composed exclusively of convolution layers and contains residual connections every 2 layers. The resolution and the number of channels of the feature maps are respectively divided and multiplied by 2 every 4 layers. After the convolutions, an average-pooling layer produces a vector of features, to which the final soft-max layer is applied to make predictions. We use the variant ResNet proposed by He et al. [28].

The ResNet-LSTM. This model is the combination of the ResNet model with an LSTM [29]. The LSTM model has been designed to model sequences and has been successfully applied in tasks such as speech recognition [30]. Pre-activations of the penultimate layer of ResNet are used as a feature vector and are passed to a bi-directional two-layer LSTM that models the evolution through time steps. The size of each hidden unit is 1024. A linear layer after the LSTM calculates the class scores for each image.

The ResNet-3D [31] is a variant of ResNet designed for the classification of image sequences. This model processes the image sequence by merging temporal

information at all layers in the network, allowing both late and early merging of information. For this application, the max-pooling and stride parameters are set to 1 in the temporal dimension. The removal of temporal aggregation is necessary to obtain one prediction per frame in the input sequence. We use the variant ‘R2plus1d-18’ proposed by Hara et al. [31].

2.3 Metrics

Several metrics are defined to evaluate the models in our context. The first metric we introduce is the Pearson product-moment r . It measures the correlation between the predicted transition time and the actual time of the corresponding transition. Before being computed, it requires applying the Viterbi algorithm beforehand so that predictions of the models are made consistent throughout the video, as is often done in the literature [19, 21, 22, 32]. The models we used do not have a strong constraint forcing them to respect the chronology of embryo development phases and can sometimes predict biologically impossible events like backward transitions ($p3 \rightarrow p2$, $pM \rightarrow p9+$, etc.). The Viterbi algorithm makes the prediction consistent by combining the transition probabilities produced by the model with the knowledge of actual biologically possible transitions. Once the predictions are made biologically plausible, we compute the correlation r between the timings predicted by the models and the actual timings:

$$r = \frac{C}{V_p \times V_{gt}}, \quad (1)$$

, where C , V_p , and V_{gt} are respectively the covariance between the predicted and actual transition times, the variance of the predicted times, and the variance of the actual times. For this metric, only the transitions present in both ground-truth and predictions are taken into account. We determined that this metric is positively biased, which led us to introduce three more metrics: the accuracy p , the Viterbi accuracy, and the temporal accuracy. The accuracy p is one of the most widely used metrics in image classification and is calculated by the proportion of images correctly labeled by the model:

$$p = \frac{N}{N_{total}}, \quad (2)$$

where N and N_{total} are respectively the numbers of images correctly classified and the total number of images. We also define a variant, the Viterbi accuracy p_v that consists in applying the Viterbi algorithm beforehand to make the prediction consistent. We use the following formula :

$$p_v = \frac{N_v}{N_{total}} \quad (3)$$

where N_v is the number of correctly classified images once the raw predictions have been refined using the Viterbi algorithm.

Finally, we define the temporal accuracy p_t as the average proportion of phase transitions that are predicted sufficiently close to the corresponding actual transition. By “close enough”, we mean that the time between the predicted transition time and the actual transition time is inferior to a threshold. Therefore, it requires that the predictions are made consistent using the Viterbi algorithm. This metric is computed as follows :

$$p_t = \frac{T - T_{far}}{T}, \quad (4)$$

where T is the total number of phase transitions and T_{far} is the number of transitions predicted too far away in time from their actual timing.

For example, consider a video containing $T = 6$ transitions ($p_2 \rightarrow p_3 \rightarrow p_4 \rightarrow p_5 \rightarrow p_6 \rightarrow p_7 \rightarrow p_8$) where the model has predicted the sequence ($p_2 \rightarrow p_3 \rightarrow p_4 \rightarrow p_5 \rightarrow p_6 \rightarrow p_8$). The model has skipped phase p_7 but has predicted phase p_8 and this is likely due to the length of phase p_7 which can be very short. As, in reality, the embryo cannot skip phase (the fact that some phases cannot be seen in the video is due to the large time interval between successive images), we consider that the model has implicitly predicted p_7 with the same timestamp as the one predicted for p_8 . Now, let's say the transitions ($p_2 \rightarrow p_3$) and ($p_3 \rightarrow p_4$) are predicted too far away from the corresponding transitions, i.e. the first image where the model has assigned the label of the new phase and the actual image corresponding to the new phase are separated by a time interval superior to a threshold θ . Then, we have $T_{far} = 2$ and the temporal precision is $p_t = (6 - 2)/6 = 0.67$.

The threshold θ needs to be dependent on the phase because some phases are more difficult to locate precisely in time than others. For this, we use intra-operator standard deviations extracted from Martínez-Granados et al. to have thresholds that are more or less large according to the intrinsic ambiguity of each phase [33]. In this work, the authors have sent time-lapse videos of embryo development to several IVF centers as an external quality control program and notably studied the intra-operator variance. Using their supplementary data, we compute the standard deviation σ_p observed between operators for each phase p . The threshold θ_p we use for phase p is simply set to σ_p .

The standard deviations for each phase are available in table 2. The p and p_v metrics have the disadvantage of penalizing models that offer phase transitions far from true transitions as much as those that are wrong by only a few frames. The temporal accuracy metric takes this into account: a model that predicts a phase change close to the actual phase change is favored over a model that is far from the truth.

2.4 Experimental setup

To show the potential use of this dataset we trained several deep neural networks on our dataset and evaluated them using cross-validation ($k = 8$). Details of the experiments are given below.

Phase	pPNa	pPNf	p2	p3	p4	p5	p6
σ_p	1.13	0.50	0.91	1.81	1.34	1.49	1.61
Phase	p7	p8	p9+	pM	pSB	pB	pEB
σ_p	2.93	5.36	4.42	5.46	3.78	3.29	4.85

Table 2: Inter-operator standard deviation of annotations in hours. Computed using data from [33].

Pre-processing and video selections. No data augmentation was used. Images were reduced from 500×500 to 224×224 to reduce GPU memory usage, as is usually done for deep learning models [11].

Some embryos grow slowly and the recording of the video only lasts a fixed amount of time, making the early phases over-represented. To prevent the model from being too biased towards early phases, we kept only the videos showing at least 6 distinct stages of development. The final number of videos used in the experiments was 756. Meta-parameters. Each training batch is composed of 10 sequences of 4 consecutive images. The ResNet model processes each image independently and therefore reads the $10 \times 4 = 40$ images as if they were independent images. An equal input sequence number and equal sequence length for the three models allow a fair comparison. The position of the sequence in the video is chosen randomly in the video. The loss function was optimized with SGD, with a constant learning rate of 0.001 and a momentum of 0.9. We applied dropout [34] ($p = 0.50$) on the last layer of each model during training.

During test and validation, to reduce GPU memory usage, the evaluation batch size was set to 150. The models were not evaluated over the entire video at once but over 150-frame sequences. Since each video contains about 500 frames, a few inferences are sufficient to analyze an entire video. Let N be the total number of training frames and L be the number of frames in a sequence. An epoch ends when the model has seen N/L sequences. To select the sequences, we used uniform random sampling with replacement, i.e. the model may see the same image several times and may not see some images within an epoch. For each split, we used 664, 47, and 45 videos for training, validation, and test. This represents respectively 297k, 20k, and 20k images and allows to detect an absolute variation of 1.5% during evaluation, with a base accuracy ranging from 65% to 70%, a significance level of 0.05, and a power of 0.9, according to a power test.

A model is trained during 100 epochs. The best model considering the validation set is then restored and evaluated on the test set.

Initializing weights. The ResNet and ResNet-3D weights are pre-trained on ImageNet [11] and Kinetics [31] respectively. The weights of the ResNet component of ResNet-LSTM are also pre-trained on ImageNet and the weights of the LSTM components are initialized randomly.

3 Results

Compiling a fully annotated, open dataset To fill an important gap in the implementation of deep learning in IVF, we sought to build an open resource of fully annotated images of human preimplantation development. The dataset contains 756 videos with annotations for 16 morphokinetic events, covering the whole development of the embryo from day 1 to day 5-6 (Figure 2). This is accompanied by 4 custom evaluation metrics and 3 baseline model performances, along with cross-validation splits to reproduce our results and to rigorously evaluate new models and methods.

Deep learning models are heavily dependent on data and might provide poor performance on a specific class if the amount of input corresponding to it is too small. This is why for each phase, we provide at least several thousand images, even for short phases like pNf, p3, or p5, (fig. 3 (a)). The only exception is pHB as it is difficult to capture, the time-lapse recording being often interrupted before reaching that stage. Nevertheless, we still provide more than a hundred images for this phase. Most videos have at least 8 annotated phases and that approximately 380 videos have more than 13 phases annotated, illustrating the richness of annotation of our dataset (fig. 3 (b)).

Sample images allow one to have a clear view of the content of the dataset and the annotations associated with the images (fig. 4). Note that, depending on their position in the well, embryos can sometimes be partially occluded which is quite common in time-lapse videos. However, even when a part of the embryo is hidden, the images are sufficient to identify the development phase. The behavior of the AI-based model on a specific type of input (like partial views/artifacts) is conditioned on its presence/absence in the training set. In our study, such events were included in the training set, the model was therefore theoretically not affected by these outlier images.

Using the API provided by Vitrolife, we could extract full-length videos and all focal planes available, highlighting the importance of data accessibility. The annotations made by experts recapitulate embryo development from tPB2 to tHB instead of focusing solely on early cleavages (t2 to t5+), as is done usually in the literature. Finally, 526 videos of our dataset correspond to embryos that were evaluated as compatible with clinical use, i.e. transferred or frozen, which are accompanied by a detailed outcome annotation (results of HCG test, presence/absence of fetal heartbeat, gestational sacs, and live-born information). This means our dataset can also be used by researchers to evaluate outcome prediction models and test cross-center generalizability. Note that the outcome information is considered as patient information, and therefore requires an agreement (MTA) with the University-Hospital of Nantes (see authors for details).

Baseline model training The first task to implement deep-learning on a dataset is to train baseline models with the most popular deep-learning architectures. The metrics associated with ResNet, ResNet-LSTM, and ResNet-3D analysis of our dataset are compiled in table 3.

Model	Split	r	p	p_v	p_t
ResNet	1	<u>0.958</u>	0.645	0.687	0.284
	2	0.894	0.57	0.594	0.292
	3	0.964	<u>0.668</u>	<u>0.698</u>	0.423
	4	0.976	0.655	0.708	0.447
	5	0.968	0.707	0.732	0.469
	6	0.981	0.702	0.747	<u>0.365</u>
	7	0.97	0.687	0.731	0.219
	8	0.974	0.671	0.711	0.469
Mean		0.961 ± 0.026	0.663 ± 0.041	0.701 ± 0.044	0.371 ± 0.09
ResNet-LSTM	1	0.98	0.663	0.681	0.375
	2	0.96	0.592	0.591	0.625
	3	0.989	0.714	0.725	0.611
	4	0.969	0.677	<u>0.701</u>	0.851
	5	0.988	0.733	0.737	0.844
	6	0.98	0.709	0.722	0.462
	7	<u>0.976</u>	0.699	0.705	0.135
	8	0.974	<u>0.691</u>	0.703	<u>0.567</u>
Mean		0.977 ± 0.009	0.685 ± 0.041	0.696 ± 0.043	0.559 ± 0.223
ResNet-3D	1	0.981	0.687	0.703	0.486
	2	0.917	0.619	0.641	0.875
	3	<u>0.977</u>	0.711	0.743	0.75
	4	0.981	0.716	0.756	0.851
	5	0.984	0.736	0.76	0.547
	6	0.982	0.742	0.777	0.553
	7	0.959	<u>0.701</u>	<u>0.733</u>	0.469
	8	0.979	0.726	0.767	<u>0.741</u>
Mean		0.97 ± 0.021	0.705 ± 0.036	0.735 ± 0.042	0.659 ± 0.154

Table 3: Performance obtained after the 8-fold cross-validation. Each row either indicates the performance of a model on one split or the mean performance across all splits accompanied by standard deviation. r is correlation, p is accuracy, p_v is Viterbi accuracy and p_t is temporal precision. For each metric, bold indicates the best mean performance on the given metric and the underline indicates the closest value to the mean performance of the model.

The first metric we considered is the correlation metric, which is close to 1 for all deep-learning approaches. This metric is poorly informative. Indeed, one can notice the high bias and low variance of the correlation metric r that is pushing all values close to 1. This is because the predicted transitions are forced to be in a biologically plausible order after applying the Viterbi algorithm, implying a minimum level of alignment with the actual transitions, hence the high correlation values. To get a better idea of the performance of the deep learning algorithms, we focused our analysis on other metrics. The accuracy provides a

greater range of values and shows that ResNet, ResNet-LSTM, and ResNet-3D are respectively able to correctly classify on average 66.3%, 68.5%, and 70.5% of the images of the test videos. Logically, the accuracy with Viterbi p_v yields higher values than the regular accuracy p because the model’s predictions are first made biologically plausible. Finally, the temporal precision shows that ResNet, ResNet-LSTM, and ResNet-3D predict respectively 37.1%, 55.9%, and 65.9% of the transitions at a timing close from the real one. These 3 metrics highlight the superiority of ResNet-LSTM and ResNet-3D over ResNet. This is explained by the fact that ResNet processes images in an isolated manner, like an embryologist having a static view of the embryo using a microscope, whereas ResNet-LSTM and ResNet-3D process several images together, like an embryologist using a TLI system, and are therefore able to more accurately understand at which development phase the embryo is currently at. This highlights the relevance of proposing a dataset composed of full videos instead of isolated images, as models designed for this kind of input can improve performance. Globally, we observed that the models achieved good performance, illustrating that our dataset is sufficient in size and quality to train and evaluate deep learning models.

Comparison of deep-learning approaches with the Ad-Hoc algorithmic annotation We then sought to evaluate the performance obtained with deep learning methods with the ad-hoc method developed in our previous work [23]. Note that we did not use the p_v metric as it requires applying the Viterbi algorithm, which is not possible for the Ad-Hoc method, as it does not generate probabilities of transition but instead directly predicts the time of the transition. The p , p_v , and p_t metrics show that these DL models overperform the ad-hoc method by a large margin (0.659 vs. 0.615 on the p_t metric and 0.705 vs. 0.58 on the p metric) confirming the interest and relevance of DL for the task of automatic morpho-kinetic parameter extraction (table 4).

Model	r	p	p_v	p_t
ResNet	0.961	0.663	0.701	0.371
ResNet-LSTM	0.977	0.685	0.696	0.559
ResNet-3D	0.97	0.705	0.735	0.659
Ad-Hoc	0.973	0.580	0.580	0.615

Table 4: Performance of deep learning methods compared to our previous work [23]. Top rows indicates the mean performances of the deep learning models across all splits, bottom row indicates the mean performance of our previous ad-hoc method on the whole dataset. r is correlation, p is accuracy, p_v is Viterbi accuracy and p_t is temporal precision. For each metric, bold indicates the best mean performance on the given metric.

Comparing our deep-learning results with previous analyses To check if our models perform similarly to those found in the literature, we evaluated 2 results: the ability to identify phases from p2 to p5+ [19–22, 32, 35] and blastocyst vs

not-blastocyst [36]. When restricting the test images to early cleavages, we obtained accuracies p similar to those found in the literature: 0.86, 0.88 and 0.88 for ResNet, ResNet-LSTM and ResNet-3D vs 0.82 to 0.87 in [19–22, 32, 35] (table 5).

Model	Identification of phases from p2 to p5+	Blastocyst vs Not-blastocyst
ResNet	0.86	0.98
ResNet-LSTM	0.88	0.99
ResNet-3D	0.88	0.99

Table 5: Evaluation of deep learning methods on the identification of phases from p2 to p5+ and blastocyst vs not-blastocyst. The metric used is the accuracy p .

To test the performance of blastocyst identification, we processed the predictions made during the first evaluation and merged phases from tPB2 to tM for the non-blastocyst class and merged phases from tB up to the end for the blastocyst class. We ignored the phase pSB as it is a phase of transition to the blastocyst stage not belonging to either of the 2 groups. We obtained accuracies of 0.98, 0.99 and 0.99 vs 0.96 in [36] on blastocyst/non-blastocyst evaluation (table 5). This highlights that our database allows the models to be trained with 16 phases without being biased when reducing the settings to what can be found in the literature.

4 Discussion

In this study, we report the development and the respective performance of popular deep learning models for the annotation of a large dataset of time-lapse videos of embryo development that we propose to make publicly available for the sake of facilitated and improved further research in the field. We chose three architectures for our experiments. First, the ResNet architecture because of its simplicity and ease to train. Second, the ResNet-LSTM and the ResNet-3D architectures because they can leverage information from the temporal context. We evaluated those architectures with cross-validation and 4 metrics including 2 custom ones that we introduced. The fair performance yielded by the models here indicates that the dataset is large enough to train a deep learning model. Also, by leveraging image sequence models like ResNet-3D or ResNet-LSTM, we could improve prediction quality, highlighting the relevance of proposing full videos instead of isolated images. The good performance can be surprising as this dataset is composed of only 756 videos and video classification can be considered more data demanding than image classification. However, video classification consists in passing a sequence of images to a model and training it

to produce a single output where each video has a single label for all its images. Here, the models are also passed as a sequence of images but they are trained to produce one output per image, i.e. classify each image, and each image has its own label. This is why this problem can be considered as image classification. This dataset size (337k images) is consistent with the dataset size found in the literature, where the number of images ranges from 60k to 600k [19–22, 32, 35]. Kanakasabapathy et al. reported that inter and intra-variance were too high when more than 6 embryo developmental phases were used [36]. Contrarily, we report here for the first time the analysis of videos consisting of 16 precise developmental phases. Although some variance is also found in our work, we were able to precisely reconstitute the succession of all 16 morpho-kinetic events. Our work, therefore, goes beyond the simplified set of classes previously used, for example taking only into account early phases up to p9+ and merging phases p4 to p9+ into one class p4+. We also observed that we were able to reproduce the performance obtained in the literature using similar setups which show that our method is at least as good as the previous analyses. Another interesting part of our work is that we implemented 2 improvements to the DL approach. Firstly, we performed 8 fold cross-validation, while previous studies used a single split. Secondly, we used both 3D CNN architecture and a dedicated temporal model, which are relevant considering the temporal nature of the data, leading to improved performance. Although not evaluated up to now in the field of IVF and time-lapse videos of embryo development, the ResNet-3D architecture has been successfully used in several other medical domains such as oncology [37, 38] cardiology [39], Computerized Tomography (CT) imagery quality, [40] and neuroimaging [41, 42]. Finally, The deep learning architecture provides superior performance to our previous Ad-Hoc method [23], highlighting the relevance of a deep learning tailored dataset as a step towards machine learning assisted IVF. Moreover, 526 of the 756 videos proposed correspond to transferred embryos and can be accompanied by detailed outcome annotations, eventually allowing other researchers to use this benchmark to validate outcome prediction models. In summary, our work will have a major impact on the implementation of DL in IVF, by providing a much-needed benchmark, ultimately benefiting infertile patients with improved clinical success rates.

5 Acknowledgments

The authors would like to thank the IVF staff at the University Hospital of Nantes, and more specifically Dr. Arnaud Reignier and Mrs. Jenna Lammers for the annotation of the database. This work was funded by ANR - Next grant DL4IVF (2017) None of the authors report having competing commercial interests concerning the submitted work.

References

- [1] M. C. Inhorn and P. Patrizio, “Infertility around the globe: new thinking on gender, reproductive technologies and global movements in the 21st century,” *Human Reproduction Update*, vol. 21, no. 4, pp. 411–426, 03 2015.
- [2] A. P. Ferraretti, V. Goossens, M. Kupka, S. Bhattacharya, J. de Mouzon, J. A. Castilla, K. Erb, V. Korsak, A. Nyboe Andersen, and European IVF-Monitoring (EIM) Consortium for the European Society of Human Reproduction and Embryology (ESHRE), “Assisted reproductive technology in Europe, 2009: results generated from European registers by ESHRE,” *Human Reproduction (Oxford, England)*, vol. 28, no. 9, pp. 2318–2331, Sep. 2013.
- [3] S. Dyer, G. Chambers, J. de Mouzon, K. Nygren, F. Zegers-Hochschild, R. Mansour, O. Ishihara, M. Bunker, and G. Adamson, “International Committee for Monitoring Assisted Reproductive Technologies world report: Assisted Reproductive Technology 2008, 2009 and 2010†,” *Human Reproduction*, vol. 31, no. 7, pp. 1588–1609, 05 2016.
- [4] G. Paternot, J. Devroe, S. Debrock, T. M. D’Hooghe, and C. Spiessens, “Intra- and inter-observer analysis in the morphological assessment of early-stage embryos,” *Reproductive biology and endocrinology : RB&E*, vol. 7, pp. 105–105, Sep 2009, 19788739[pmid].
- [5] A. Storr, C. A. Venetis, S. Cooke, S. Kilani, and W. Ledger, “Inter-observer and intra-observer agreement between embryologists during selection of a single Day 5 embryo for transfer: a multicenter study,” *Human Reproduction*, vol. 32, no. 2, pp. 307–314, 01 2017.
- [6] A. E. Baxter Bendus, J. F. Mayer, S. K. Shipley, and W. H. Catherino, “Interobserver and intraobserver variation in day 3 embryo grading,” *Fertil Steril*, vol. 86, no. 6, pp. 1608–1615, Dec 2006.
- [7] C. Pribenszky, A.-M. Nilselid, and M. Montag, “Time-lapse culture with morphokinetic embryo selection improves pregnancy and live birth chances and reduces early pregnancy loss: a meta-analysis.” *Reproductive BioMedecine Online*, vol. 35, pp. 511–520, 2017.
- [8] R. J. Paulson, D. E. Reichman, N. Zaninovic, L. R. Goodman, and C. Racowsky, “Time-lapse imaging: clearly useful to both laboratory personnel and patient outcomes versus just because we can doesn’t mean we should,” *Fertility and Sterility*, vol. 109, no. 4, pp. 584–591, Apr 2018. [Online]. Available: <https://doi.org/10.1016/j.fertnstert.2018.01.042>
- [9] S. Armstrong, P. Bhide, V. Jordan, A. Pacey, J. Marjoribanks, and C. Farquhar, “Time-lapse systems for embryo incubation and assessment in assisted reproduction,” *Cochrane Database of Systematic Reviews*, no. 5,

2019. [Online]. Available: <https://doi.org/10.1002/14651858.CD011320.pub4>

[10] D. Silver, A. Huang, C. J. Maddison, A. Guez, L. Sifre, G. van den Driessche, J. Schrittwieser, I. Antonoglou, V. Panneershelvam, M. Lanctot, S. Dieleman, D. Grewe, J. Nham, N. Kalchbrenner, I. Sutskever, T. Lillicrap, M. Leach, K. Kavukcuoglu, T. Graepel, and D. Hassabis, “Mastering the game of go with deep neural networks and tree search,” *Nature*, vol. 529, no. 7587, pp. 484–489, Jan 2016. [Online]. Available: <https://doi.org/10.1038/nature16961>

[11] A. Krizhevsky, I. Sutskever, and G. E. Hinton, “Imagenet classification with deep convolutional neural networks,” in *Advances in Neural Information Processing Systems*, F. Pereira, C. J. C. Burges, L. Bottou, and K. Q. Weinberger, Eds., vol. 25. Curran Associates, Inc., 2012. [Online]. Available: <https://proceedings.neurips.cc/paper/2012/file/c399862d3b9d6b76c8436e924a68c45b-Paper.pdf>

[12] A. Vaswani, N. Shazeer, N. Parmar, J. Uszkoreit, L. Jones, A. N. Gomez, L. u. Kaiser, and I. Polosukhin, “Attention is all you need,” in *Advances in Neural Information Processing Systems*, I. Guyon, U. V. Luxburg, S. Bengio, H. Wallach, R. Fergus, S. Vishwanathan, and R. Garnett, Eds., vol. 30. Curran Associates, Inc., 2017. [Online]. Available: <https://proceedings.neurips.cc/paper/2017/file/3f5ee243547dee91fdb053c1c4a845aa-Paper.pdf>

[13] A. W. Senior, R. Evans, J. Jumper, J. Kirkpatrick, L. Sifre, T. Green, C. Qin, A. Žídek, A. W. R. Nelson, A. Bridgland, H. Penedones, S. Petersen, K. Simonyan, S. Crossan, P. Kohli, D. T. Jones, D. Silver, K. Kavukcuoglu, and D. Hassabis, “Improved protein structure prediction using potentials from deep learning,” *Nature*, vol. 577, no. 7792, pp. 706–710, Jan 2020. [Online]. Available: <https://doi.org/10.1038/s41586-019-1923-7>

[14] M. Afnan and et al., “Interpretable, not black-box, artificial intelligence should be used for embryo selection,” *Human Reproduction Open*, vol. 2021, no. 4, 11 2021, hoab040. [Online]. Available: <https://doi.org/10.1093/hropen/hoab040>

[15] A. E. Johnson, T. J. Pollard, L. Shen, L.-w. H. Lehman, M. Feng, M. Ghassemi, B. Moody, P. Szolovits, L. Anthony Celi, and R. G. Mark, “Mimic-iii, a freely accessible critical care database,” *Scientific Data*, vol. 3, no. 1, p. 160035, May 2016. [Online]. Available: <https://doi.org/10.1038/sdata.2016.35>

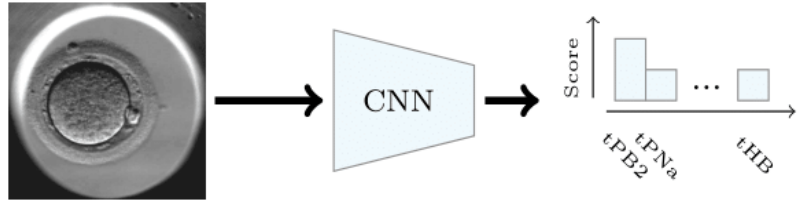
[16] N. A. Phillips, P. Rajpurkar, M. Sabini, R. Krishnan, S. Zhou, A. Pareek, N. M. Phu, C. Wang, M. Jain, N. D. Du, S. Q. Truong, A. Y. Ng, and M. P. Lungren, “Chexphoto: 10,000+ photos and transformations of chest x-rays for benchmarking deep learning robustness,” 2020.

- [17] J. Staal, M. Abramoff, M. Niemeijer, M. Viergever, and B. van Ginneken, “Ridge-based vessel segmentation in color images of the retina,” *IEEE Transactions on Medical Imaging*, vol. 23, no. 4, pp. 501–509, 2004.
- [18] D. Jha, P. H. Smedsrud, M. A. Riegler, P. Halvorsen, T. de Lange, D. Johansen, and H. D. Johansen, “Kvasir-seg: A segmented polyp dataset,” in *International Conference on Multimedia Modeling*. Springer, 2020, pp. 451–462.
- [19] T. Lau, N. Ng, J. Gingold, N. Desai, J. J. McAuley, and Z. C. Lipton, “Embryo staging with weakly-supervised region selection and dynamically-decoded predictions,” *CoRR*, vol. abs/1904.04419, 2019.
- [20] J. Silva-Rodríguez, A. Colomer, M. Meseguer, and V. Naranjo, “Predicting the success of blastocyst implantation from morphokinetic parameters estimated through cnns and sum of absolute differences,” in *2019 27th European Signal Processing Conference (EUSIPCO)*, 2019, pp. 1–5.
- [21] A. Khan, S. Gould, and M. Salzmann, “Deep convolutional neural networks for human embryonic cell counting,” in *Computer Vision – ECCV 2016 Workshops*, G. Hua and H. Jégou, Eds. Cham: Springer International Publishing, 2016, pp. 339–348.
- [22] R. M. Rad, P. Saeedi, J. Au, and J. Havelock, “Blastomere cell counting and centroid localization in microscopic images of human embryo,” in *2018 IEEE 20th International Workshop on Multimedia Signal Processing (MMSP)*, 2018, pp. 1–6.
- [23] M. Feyeux, A. Reignier, M. Mocaer, J. Lammers, D. Meistermann, P. Barrière, P. Paul, L. David, and T. Fréour, “Development of automated annotation software for human embryo morphokinetics,” *Human reproduction (Oxford, England)*, 03 2020.
- [24] T. Fréour, N. Le Fleuter, J. Lammers, C. Spingart, A. Reignier, and P. Barrière, “External validation of a time-lapse prediction model,” *Fertility and Sterility*, vol. 103, no. 4, pp. 917–922, Apr 2015.
- [25] N. Basile, D. Morbeck, J. García-Velasco, F. Bronet, and M. Meseguer, “Type of culture media does not affect embryo kinetics: a time-lapse analysis of sibling oocytes,” *Human Reproduction*, vol. 28, no. 3, pp. 634–641, 2013.
- [26] A. Sunde, D. Brison, J. Dumoulin, J. Harper, K. Lundin, M. C. Magli, E. Van den Abbeel, and A. Veiga, “Time to take human embryo culture seriously†,” *Human Reproduction*, vol. 31, no. 10, pp. 2174–2182, 09 2016. [Online]. Available: <https://doi.org/10.1093/humrep/dew157>
- [27] H. N. Ciray, A. Campbell, I. E. Agerholm, J. Aguilar, S. Chamayou, M. Esbert, and f. T. T.-L. U. G. Sayed, Shabana, “Proposed guidelines on the

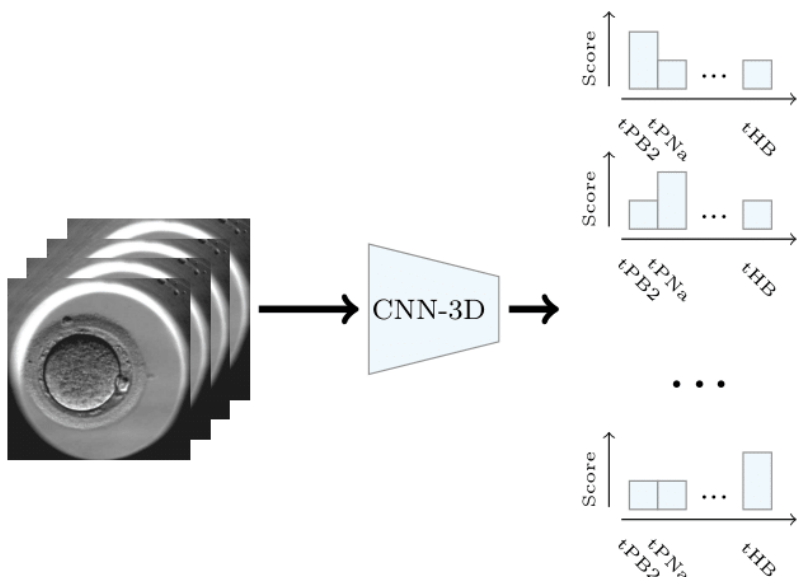
nomenclature and annotation of dynamic human embryo monitoring by a time-lapse user group,” *Human Reproduction*, vol. 29, no. 12, pp. 2650–2660, 10 2014.

- [28] K. He, X. Zhang, S. Ren, and J. Sun, “Deep residual learning for image recognition,” *CoRR*, vol. abs/1512.03385, 2015.
- [29] S. Hochreiter and J. Schmidhuber, “Long short-term memory,” *Neural Comput.*, vol. 9, no. 8, p. 1735–1780, Nov. 1997.
- [30] A. Graves, N. Jaitly, and A. Mohamed, “Hybrid speech recognition with deep bidirectional lstm,” in *2013 IEEE Workshop on Automatic Speech Recognition and Understanding*, Dec 2013, pp. 273–278.
- [31] K. Hara, H. Kataoka, and Y. Satoh, “Learning spatio-temporal features with 3d residual networks for action recognition,” 2017.
- [32] N. H. Ng, J. McAuley, J. A. Gingold, N. Desai, and Z. C. Lipton, “Predicting embryo morphokinetics in videos with late fusion nets and dynamic decoders,” 2018. [Online]. Available: <https://openreview.net/forum?id=By1QAYkvz>
- [33] L. Martínez-Granados, M. Serrano, A. González-Utor, N. Ortíz, V. Badajoz, E. Olaya, N. Prados, M. Boada, J. A. Castilla, and S. I. G. i. Q. o. A. S. S. f. t. S. of Reproductive Biology), “Inter-laboratory agreement on embryo classification and clinical decision: Conventional morphological assessment vs. time lapse,” *PloS one*, vol. 12, no. 8, pp. e0183328–e0183328, Aug 2017, 28841654[pmid]. [Online]. Available: <https://pubmed.ncbi.nlm.nih.gov/28841654>
- [34] N. Srivastava, G. Hinton, A. Krizhevsky, I. Sutskever, and R. Salakhutdinov, “Dropout: A Simple Way to Prevent Neural Networks from Overfitting,” *Journal of Machine Learning Research*, vol. 15, pp. 1929–1958, 2014.
- [35] Z. Liu, B. Huang, Y. Cui, Y. Xu, B. Zhang, L. Zhu, Y. Wang, L. Jin, and D. Wu, “Multi-task deep learning with dynamic programming for embryo early development stage classification from time-lapse videos,” 2019.
- [36] M. K. Kanakasabapathy, P. Thirumalaraju, C. L. Bormann, H. Kandula, I. Dimitriadis, I. Souter, V. Yogesh, S. Kota Sai Pavan, D. Yarravarapu, R. Gupta, R. Pooniwala, and H. Shafiee, “Development and evaluation of inexpensive automated deep learning-based imaging systems for embryology,” *Lab Chip*, vol. 19, pp. 4139–4145, 2019.
- [37] Z. Yuan, T. Xu, J. Cai, Y. Zhao, W. Cao, A. Fichera, X. Liu, J. Yao, and H. Wang, “Development and validation of an image-based deep learning algorithm for detection of synchronous peritoneal carcinomatosis in colorectal cancer,” *Annals of surgery*, Jul 2020. [Online]. Available: <http://europepmc.org/abstract/MED/32694449>

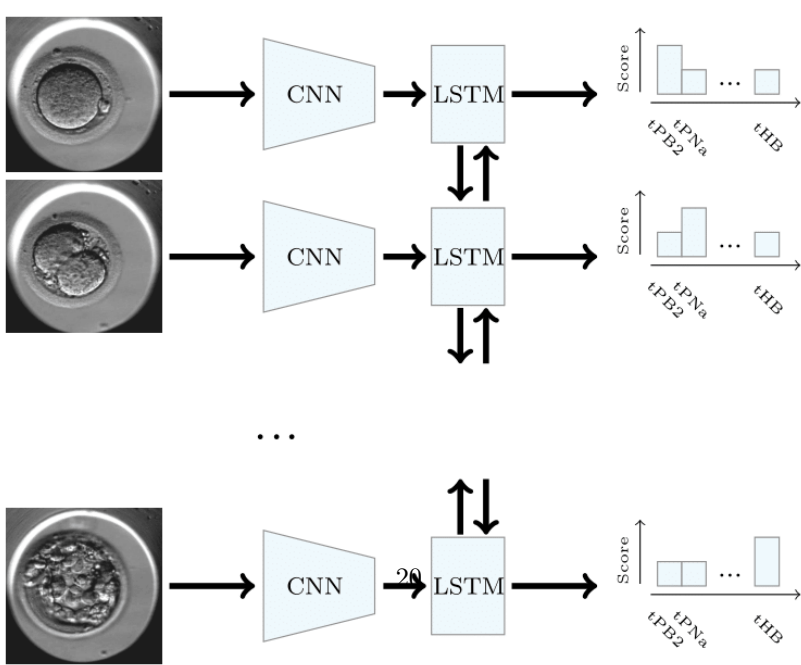
- [38] L. Schmarje, C. Zelenka, U. Geisen, C.-C. Glüer, and R. Koch, “2d and 3d segmentation of uncertain local collagen fiber orientations in shg microscopy,” in *Pattern Recognition*, G. A. Fink, S. Frintrop, and X. Jiang, Eds. Cham: Springer International Publishing, 2019, pp. 374–386.
- [39] C. He, J. Wang, Y. Yin, and Z. Li, “Automated classification of coronary plaque calcification in OCT pullbacks with 3D deep neural networks,” *Journal of Biomedical Optics*, vol. 25, no. 9, pp. 1 – 13, 2020. [Online]. Available: <https://doi.org/10.1117/1.JBO.25.9.095003>
- [40] D. Choi, J. Kim, S.-H. Chae, B. Kim, J. Baek, A. Maier, R. Fahrig, H.-S. Park, and J.-H. Choi, “Multidimensional noise reduction in c-arm cone-beam ct via 2d-based landweber iteration and 3d-based deep neural networks,” in *Medical Imaging 2019: Physics of Medical Imaging*, vol. 10948. International Society for Optics and Photonics, 2019, p. 1094837.
- [41] Y. Shmulev and M. Belyaev, “Predicting conversion of mild cognitive impairments to alzheimer’s disease and exploring impact of neuroimaging,” in *Graphs in Biomedical Image Analysis and Integrating Medical Imaging and Non-Imaging Modalities*, D. Stoyanov, Z. Taylor, E. Ferrante, A. V. Dalca, A. Martel, L. Maier-Hein, S. Parisot, A. Sotiras, B. Papiez, M. R. Sabuncu, and L. Shen, Eds. Cham: Springer International Publishing, 2018, pp. 83–91.
- [42] S. Han, Y. Zhang, Y. Ren, J. Posner, S. Yoo, and J. Cha, “3D distributed deep learning framework for prediction of human intelligence from brain MRI,” in *Medical Imaging 2020: Biomedical Applications in Molecular, Structural, and Functional Imaging*, A. Krol and B. S. Gimi, Eds., vol. 11317, International Society for Optics and Photonics. SPIE, 2020, pp. 484 – 490. [Online]. Available: <https://doi.org/10.1117/12.2549758>



(a) The ResNet model



(b) The ResNet-3D model



(c) The ResNet-LSTM model

Figure 1: The different models evaluated. ResNet takes an isolated image as input and outputs a vector of class probabilities. ResNet-LSTM and ResNet-3D have as input a short sequence of images and output a sequence of probability

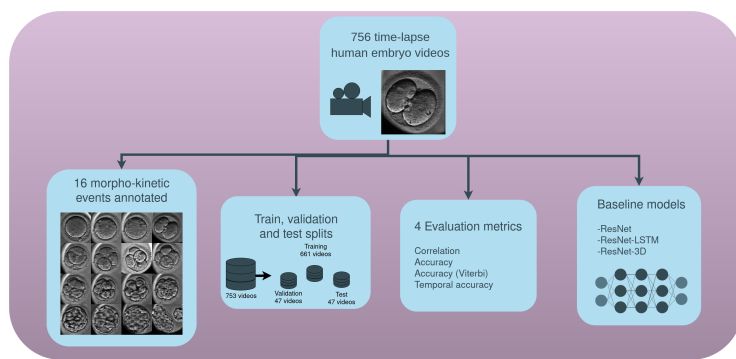
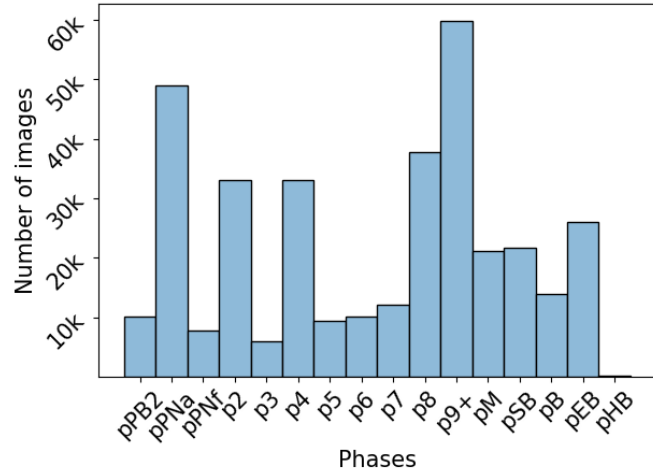
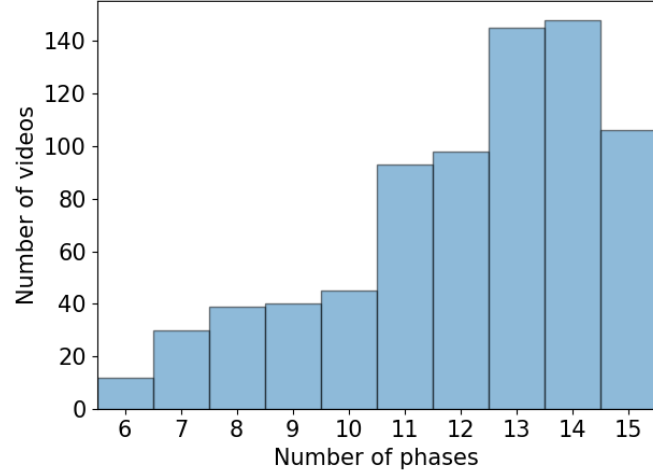


Figure 2: The time-lapse embryo dataset. This dataset contains 756 videos with annotations for 16 morpho-kinetic events, accompanied by 4 custom evaluation metrics and 3 baseline model performances, along with cross-validation splits.



(a)



(b)

Figure 3: Statistics of the dataset. (a) The number of images per phase in the dataset. (b) The number of phases per video in the dataset.

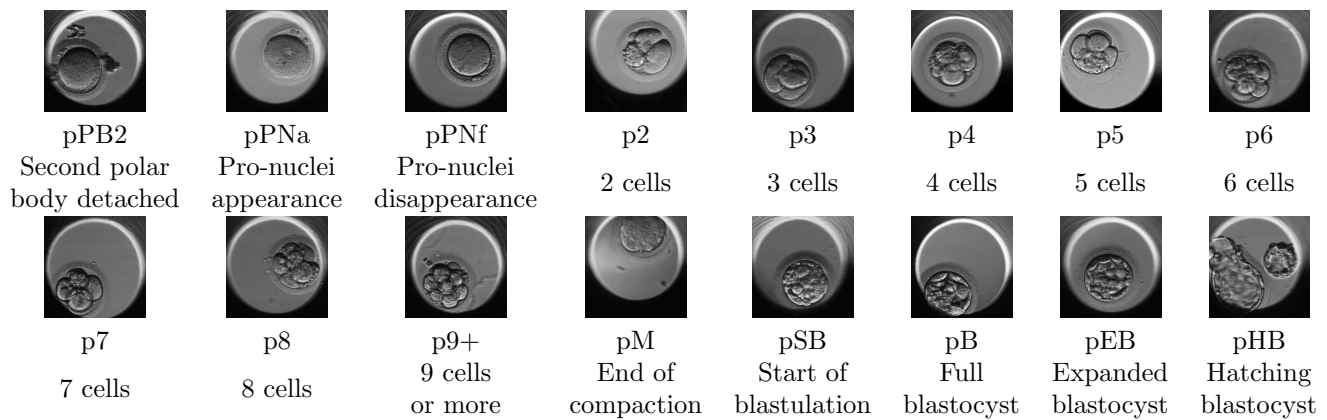


Figure 4: Illustrations of the 16 development phases used. Contrast and luminosity are standardized for better visualization.